We are IntechOpen, the world's leading publisher of Open Access books
Built by scientists, for scientists

6,900
Open access books available

185,000
International authors and editors

200M
Downloads

154
Countries delivered to

Our authors are among the

TOP 1%
most cited scientists

12.2%
Contributors from top 500 universities

CLARIVATE ANALYTICS
BOOK CITATION INDEX
INDEXED

WEB OF SCIENCE™

Selection of our books indexed in the Book Citation Index
in Web of Science™ Core Collection (BKCI)

Interested in publishing with us?
Contact book.department@intechopen.com

Numbers displayed above are based on latest data collected.
For more information visit www.intechopen.com

Interferometry Applications in All-Optical Communications Networks

Rogerio Pais Dionisio

Additional information is available at the end of the chapter

Abstract

Throughout the years, the expanded search and flow of information led to an expansion of traffic intensity in today's optical communication systems. Coherent communications, using the amplitude and phase of the optical wave, resurface as one of the transmission methods to increase the effective bandwidth of optical channels. In this framework, this chapter presents a study on all-optical format conversion of modulated signals, using exclusively interferometric techniques through wavelength conversion, based on Mach-Zehnder interferometers with semiconductor optical amplifiers (MZI-SOA). This technique, when applied in interconnection nodes between optical networks with different bit rates and modulation formats, allows a better efficiency and scalability of the network. The chapter presents an experimental characterization of the static and dynamic properties of the MZI-SOA and explores all-optical techniques for the conversion from amplitude modulation to phase modulation. Finally, it briefly presents the potential of MZI-SOAs for the conversion of amplitude signals to more advanced modulation formats, such as quadrature phase shift keying (QPSK) and quadrature amplitude modulation (QAM) signals.

Keywords: all-optical networks, signal processing, Mach-Zehnder interferometer

1. Introduction

From the exponential popularity of Internet and its derived new services, recently deployed communication networks should be capable to provide more information throughput than ever. On a recent study [1], CISCO has estimated that global Internet traffic has increased by a factor of height over the past five years and will increase nearly by a factor of four over the

next five years, with an annual global Internet protocol (IP) traffic exceeding the tens of zettabyte mark by the end of 2017.

High definition (HD) streaming video and peer-to-peer applications use the majority of bandwidth in most broadband networks today. When we add the bandwidth requirements of online social networks, Internet browsing or online gaming, broadband service providers have to supply an increasingly larger amount of bandwidth. Besides human-made Internet traffic, machine-to-machine (M2M) communications [2], fostered by smart city applications [3] and the opening of new radio channel opportunities [4] are spreading globally. The Internet of things (IOT) [5] will contribute even more to increase the quantity of data exchanged in communication networks, and especially on optical communication networks, used both by wireless and cable communications.

Photonics technologies have largely contribute to the considerable development of telecommunication networks, since they appearance 30 years ago, and one can predict that they will serve as ground for most of the network revolutions still to come. A recent study [6] of the drivers of photonics suggests that its future development will be made along four main paths: to make optical networks faster, more transparent, more dynamic and greener. With current technology, it may be difficult to follow simultaneously all four path, which is a major constrain to implement a novel generation of optical networks. However, these difficulties may be relieved by recent developments in the field of wavelength conversion, all-optical signal processing and flexible techniques to generate enhanced modulation formats in optical signals.

In this context, this chapter presents several techniques on format conversion of modulated signals, using Mach-Zehnder interferometers with semiconductor optical amplifiers (MZI-SOA). The MZI-SOA show very attractive properties, and therefore, the goal is to investigate their potential as an optical node for the dynamic conversion and generation of optical signals. As such, two techniques to implement all-optical modulation format conversion are explored. These techniques, when applied in interconnection nodes between different optical networks with variable bit rates and modulation systems, allow a better efficiency and scalability of the network.

2. MZI-SOA features

This section presents an experimental methodology to study the static and dynamic properties of the MZI-SOA. The device under test is a commercial hybrid-integrated device, manufactured by the centre for integrated photonics (CIP) [7], consisting of a passive, planar silica balanced MZI with nonlinear SOAs and phase shifters (PSs) assembled in each interferometer arm. Sections 2.1 and 2.2 describe the characterization of active and passive components of the MZI-SOA, in static operational conditions. The methodology uses simple optical power measurements to extract operative parameters. Then, section 2.3 investigates the dynamic properties of the MZI-SOA as an optical gate. Overall conclusions about this topic are presented at the end.

2.1. Static properties

MZI-SOAs are devices with a small footprint, but a huge potential for application in many optical domains. They can be used in optical gates [8], digital phase and amplitude modulation [9], wavelength conversion and switching [10], signal regeneration and all-optical processing [11], among others. In all these applications, the operational parameters of MZI-SOA active elements (SOA and PSs) must be previously calibrated, to set an optimal setting point in terms of power/phase variations and mean output power, according to the available inputs and the expected application. The majority of the biasing point procedures require extensive and complex initial setup stage, which changes from device to device, due to their intrinsic production yields.

Figure 1 show a photograph of the MZI-SOA under test in this experimental study. The package contains two MZI-SOA structures on a single chip [12]. The MZI-SOA is hybridly incorporated with a silica substrate (motherboard) that contains the optical waveguides, such as Y junctions and couplers; the SOAs are built-in on an independent silicon board, which is passively assembled in the motherboard; the active elements, i.e. the PSs and the SOAs, are assembled in the daughterboard; a Vgroove to simplify fibre pigtailing of the motherboard [13]. MZI-SOA with hybrid integration result in more flexibility but increased yields, where each active and passive element has its own asymmetries and tolerances (e.g. asymmetric splitting ratio of the couplers). These issues have various implications in some MZI-SOA functionalities, for example, on the maximization of extinction ratio (ER) between the output ports. For experimental testing, the chip was installed on a prototype box that included SOA current and phase shifter voltage electronics together with temperature control. A temperature control system takes measurements from a thermistor and actuates on a Peltier cell to keep the chip temperature constant at the desired value. All measurements were made at a temperature of 25°C.
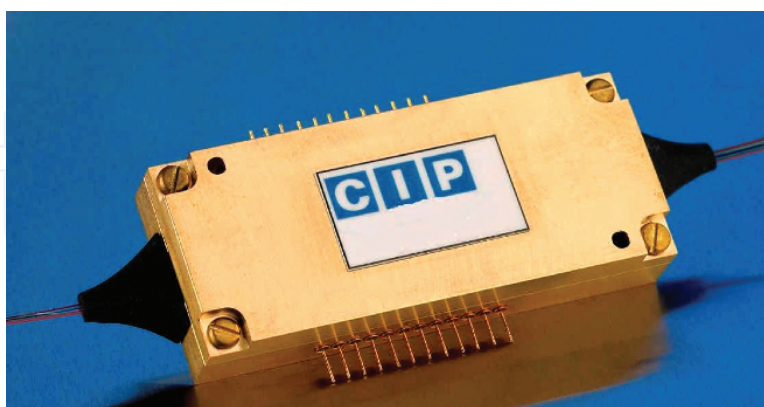

Figure 1. Twin MZI-SOA device used for experimental measurements. A strip of eight fibres enters the MZI-SOAs on the right (four fibres per MZI-SOA), and a strip of four fibre exits on the left (two fibres per MZI-SOA).

Due to the interferometric configuration of the MZI-SOA, the power distribution along the interferometer arms will affect the interference strength at the output and its eventual optimization. Thus, it is essential to characterize all passive parts. To execute the experimental

analysis on the device asymmetry, we use the setup depicted in **Figure 2**. Each arm of the MZI incorporates one SOA and one PS. For each input-output path, two sets of switches are used, as seen in **Figure 2**. This configuration allows measurements of the gain of one of the arms when the other arm is blocked by a switched off SOA, and the SOA gain dependence on the biasing current.
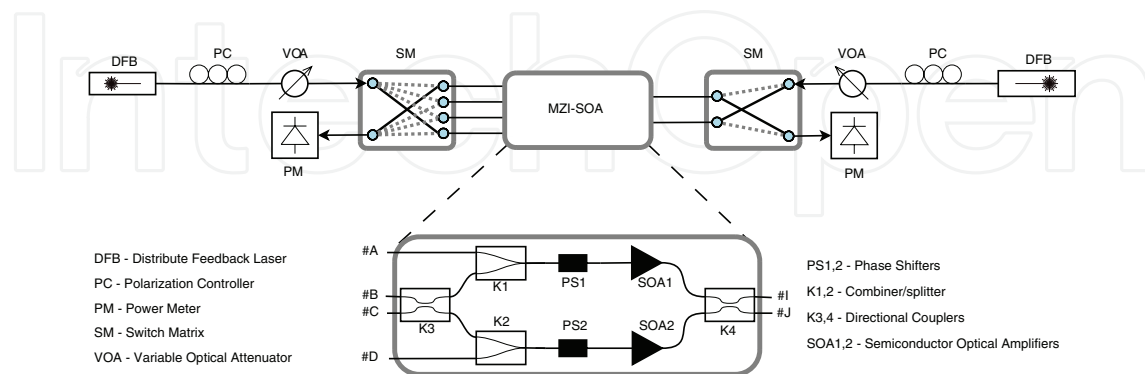

Figure 2. Experimental setup used to characterize the MZI-SOA with power measurements.

A distributed feed-back (DFB) laser with wavelength 1546.12 nm is used as the input signal and will be kept fixed in all upcoming experimental tests (The wavelength was chosen according to the MZI-SOA manufacturer specifications). All power measurements were obtained through a power meter (PM).

2.1.1. Internal couplers

In order to carry out the analysis of all MZI-SOA internal couplers, and their asymmetry properties, each input-output path is analysed independently, biasing one SOA at time accordingly to the path. For all coupling factor measurements, continuous wave (CW) laser input power is constant at 3 dBm. When simply biased, the SOAs current value is set to 200 mA. PS1 and PS2 are always switched off, with voltage source = 0 V, since a PS has little impact on couplers characterization, and only one SOA is biased at each measurement.
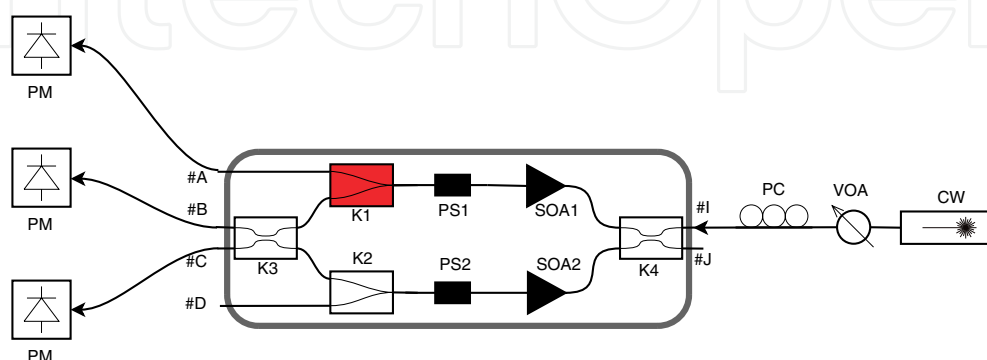

Figure 3. Setup for the characterization of K1 coupling factor.

Coupling factor of coupler K1 is characterized using the setup depicted in **Figure 3**. SOA1 is biased at 200 mA and SOA2 is switched off, i.e. with 0 mA current.

Port #I is used as the input, but port #J could also be used as well. Power measurements must be carried out at ports #A, #B and #C, with a PM. Coupling factor α_1 is obtained as

$$\alpha_1 = \frac{P_{\#A}}{\left(P_{\#A} + P_{\#B} + P_{\#C} \right)} \tag{1}$$

using a linear scale to express power values.

With SOA1 unbiased (0 mA) and SOA2 biased at 200 mA, K2 coupling factor is measured when light is injected through MZI-SOA port #J and optical power measurements are made at ports #B, #C and #D, as depicted in **Figure 4**.
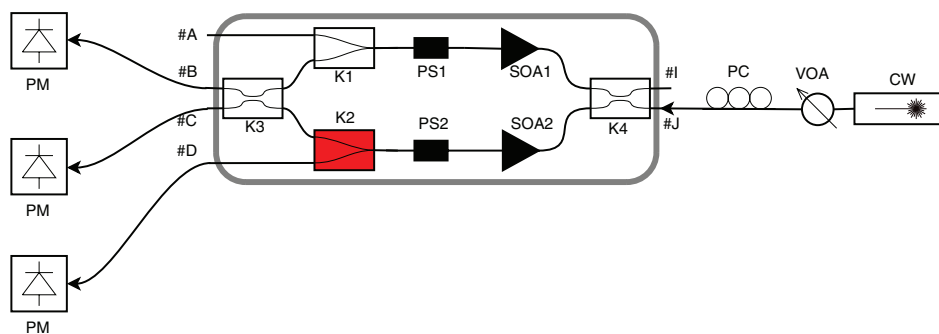

Figure 4. Setup for the characterization of K2 coupling factor.

Coupling factor α_2 is computed as,

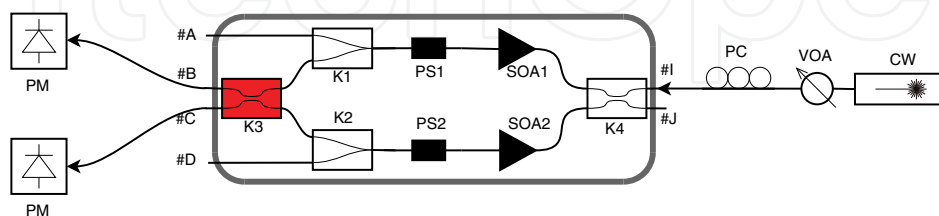$$\alpha_2 = \frac{P_{\#D}}{\left(P_{\#B} + P_{\#C} + P_{\#D} \right)}. \tag{2}$$

Figure 5. Setup for the characterization of K3 coupling factor.

The coupling factor of coupler K3 is computed from two power measurements, at port #B and port #C, as shown in **Figure 5**. Either SOA1 or SOA2 could be biased at 200 mA, but one SOA must be switched off.

Input power can be injected from port #I or port #J. Coupling factor α_3 is obtained through the following expression,

$$\alpha_3 = \frac{P_{\#B}}{\left(P_{\#B} + P_{\#C}\right)}.$$ (3)

At last, K4 coupling factor calculation follows the setup depicted in **Figure 6**. When the input optical power is injected on Port #D, then we should bias SOA2, and SOA1 should remain unbiased. If the selected input is port #A, then SOA1 should be biased and SOA2 switched off. If the input is either port #B or #C, then anyone of the two SOAs can be used.
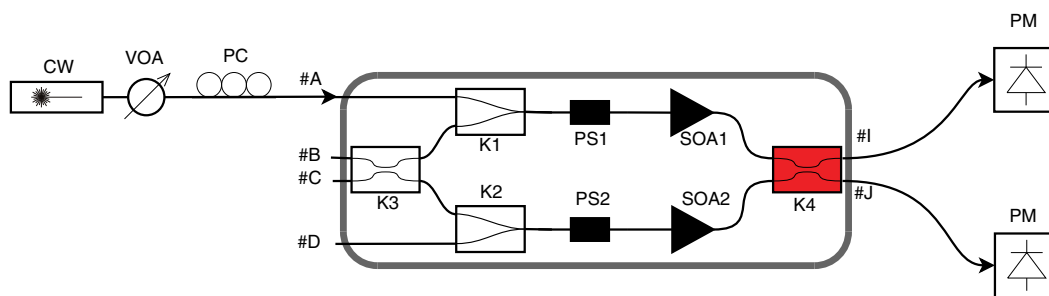

Figure 6. Setup for the characterization of K4 coupling factor.

Power measurement is taken at ports #I and #J. Coupling factor α_4 is given by,

$$\alpha_4 = \frac{p_{\#I}}{\left(p_{\#I} + p_{\#J}\right)}.$$ (4)

From the measurement results presented in **Table 1**, we conclude that couplers are not symmetrical, as ideally would be expected on this device. Furthermore, splitting factors are all different. This asymmetry induces an uneven power distribution along the interferometer arms that in any operational point will cause side effects, such as different saturation levels of the SOAs from each arm.

Coupler	CW port	PM port	I_{SOA1}	I_{SOA2}	Formulation	Value
K1	#I	#A, #B, #C	200 mA	0 mA	Eq. (1)	52%
K2	#J	#B, #C, #D	0 mA	200 mA	Eq. (2)	42%
K3	#I	#B, #C	200 mA	0 mA	Eq. (3)	52%
K4	#A	#I, #J	200 mA	0 mA	Eq. (4)	60%

Table 1. Procedure for measurements and calculations.

From here, we can observe the coupling factor of all passive couplers inside the interferometric structure and compute the overall asymmetry on the power distribution along the interferometer arms.

2.1.2. SOA

The next stage of the interferometer characterization is the analysis of SOA output power dependence on input power and SOA bias current. These measurements were realized, considering the two arms individually, first with a light path from input #B to output #J and SOA1 unbiased; then, with a light path from input #A to output #I and SOA2 unbiased, as depicted, respectively, in **Figures 7** and **8**. It is important to emphasize that this analysis refers to the whole light path where the optical wave propagates, so it includes all power losses and any other type of asymmetry of the interferometer chip.
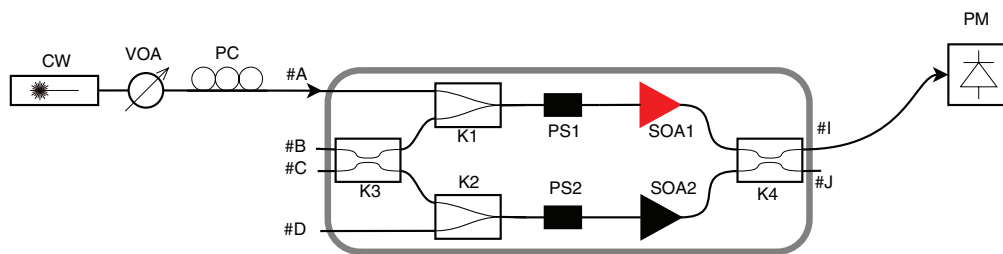

Figure 7. Setup for the characterization of SOA1.
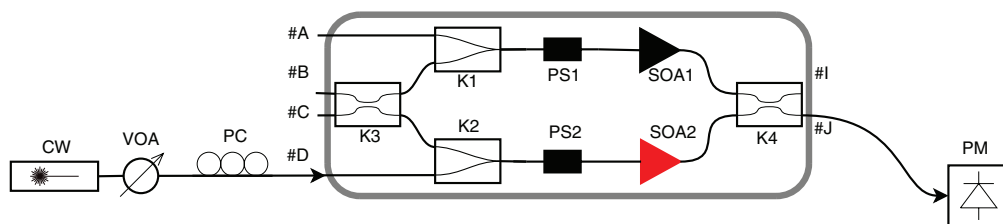

Figure 8. Setup for the characterization of SOA2.

For the evaluation of the SOA dependence from bias current, the injected power of CW power is set previously at a low value and the bias current is swept from 150 to 400 mA. For each current step, the optical power value on the output port is first measured and then saved. Then, input power is gradually increased, respecting the maximum permissible power given by the device specifications, and the previous process and measurements are repeated. **Figure 9** shows the results of the dependence of the SOA output power as a function of the SOA bias current.

To characterize the influence of the input power on the SOA gain, the power of a CW laser is gradually increased from 1 to 10 mW, while the SOA bias current is kept constant. The output power is then recorded for each measurement. From **Figure 10**, we observe the SOA output power dependence on the input power, for both SOAs and several bias currents. From the

resulting curves, we obtain the necessary setting points (input power and SOA bias) when the SOA gain begin to saturate.
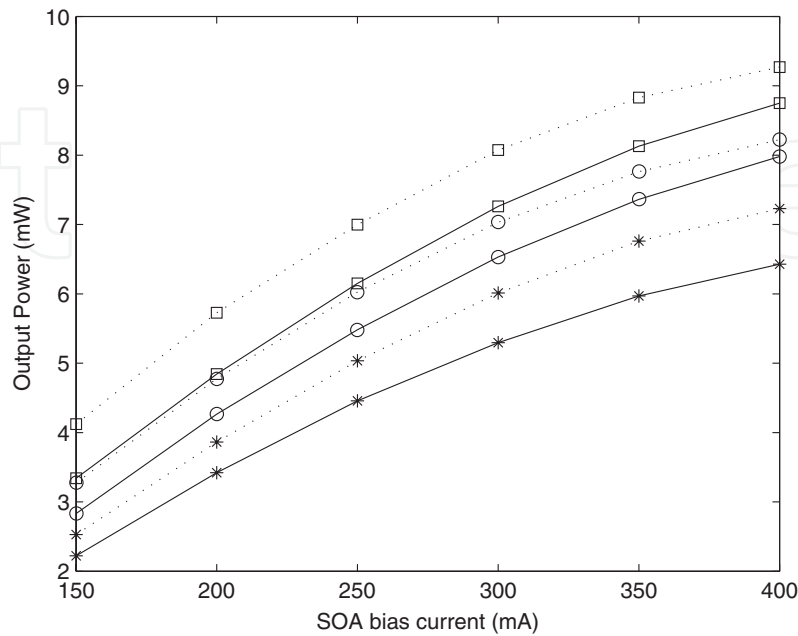

Figure 9. MZI-SOA output power at port #I (full line) and #J (dashed line), as a function of SOA1 and SOA2 bias current, respectively. Input power equal to −8, −2 and 10 dBm (asterisks, circles and squares, respectively). The lines are guides for the eyes.
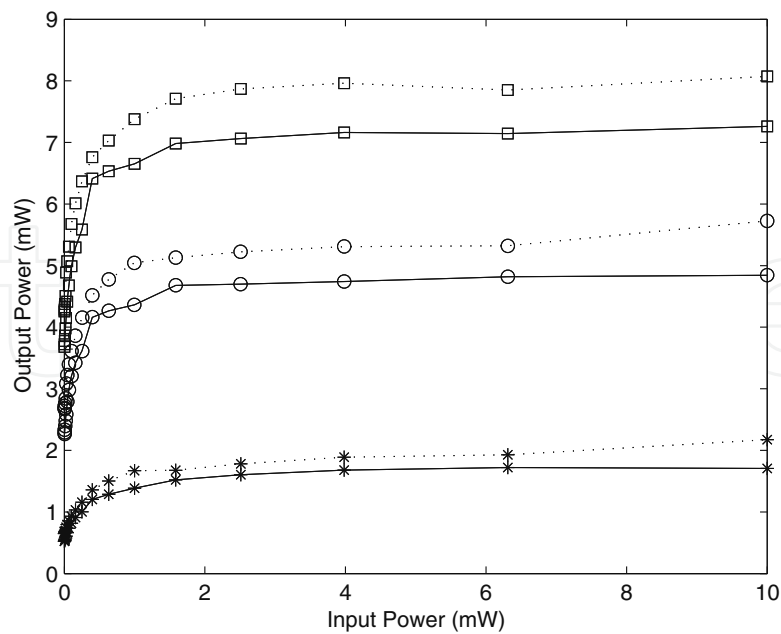

Figure 10. MZI-SOA output power at port #J (dashed line) and port #I (full line), vs. input CW power at ports #D and #A, respectively. SOA bias currents are adjusted to 100, 200 and 300 mA (asterisks, circles and squares, respectively). The lines are guides for the eyes.

2.1.3. Extinction ratio characterization

The power at each output ports of the MZI-SOAs under test (ports #I and #J) is a result of an interference process taking place in coupler K4. The intensity and phase of the optical signal of coupler K4 inputs will set the conditions for the measured outputs. In particular, when used as an intensity modulator, one key factor to take into account is the ER between the output signals. By definition, the ER is the ratio of the optical power levels measured at output ports #J and #I,

$$ER = 10 \log_{10}\left(\frac{P_{\#I}}{P_{\#J}} \right). \tag{5}$$

The ER value is given in dB and power $P_{\#I}$ and $P_{\#J}$ are given on a linear scale.

As an example, the power distribution on the MZI-SOA internal waveguides can be varied even more, through SOAs current variation, leading to the subsequent change of the interference settings on coupler K4. To observe the effect of bias currents on the ER, we employ the setup from **Figure 11**. Port #B receives a CW signal, and both PSs of the MZI-SOA remains unbiased (voltage set to 0 V).
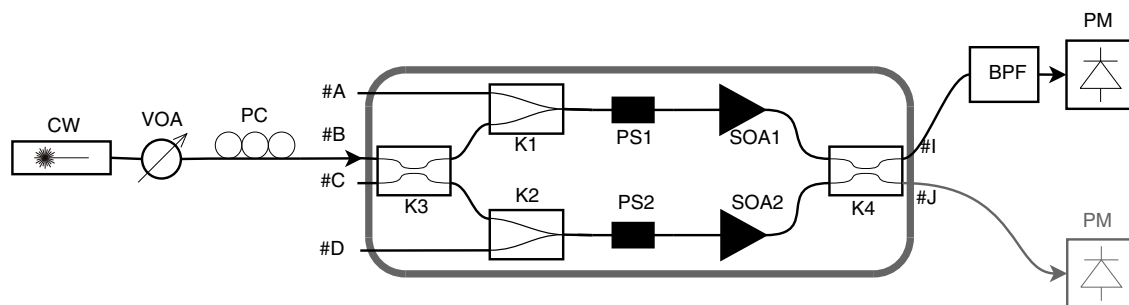

Figure 11. Setup for the characterization of ER dependence on bias current.

In **Figure 12**, we observe the dynamic of both the constructive and destructive interference, respectively, at the output port #J and #I, by gradually increasing SOA1 bias current, with SOA2 current constant at a reference value (200 mA).

This process is repeated with SOA1 bias current constant at 200 mA, while SOA2 current is swept, using a CW laser beam connected at input port #B. With this methodology and after measuring the power at the output port #I and #J, we observe in **Figure 11** that there is a misalignment between #J and #I maximum and minimum power levels. This is caused by the gain variation in the SOA with the varying bias current, together with the asymmetrical coupling factors of the couplers and the phase shift of the electromagnetic field. The best operational point, without phase shifters corrections, is established searching for SOA1 bias current for the maximum ER.
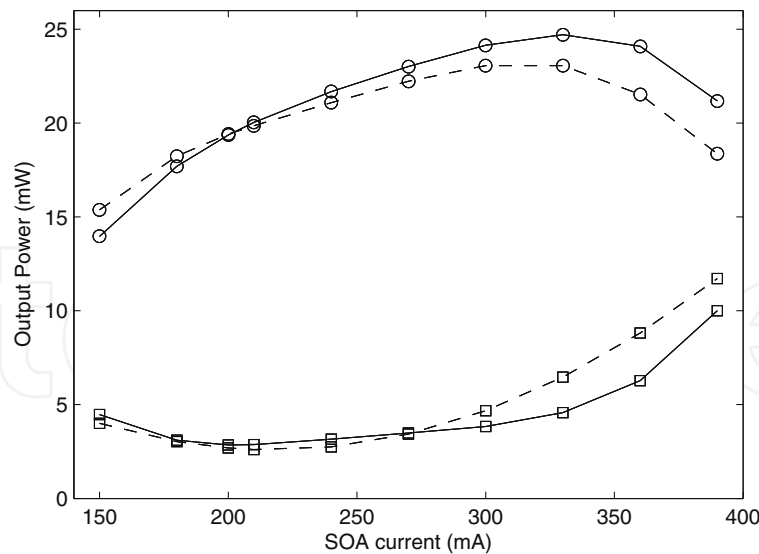
Figure 12. MZI-SOA output power at port #I (squares) and port #J (circles), as a function of SOA1 (dashed line) and SOA2 (full line) bias current. Input power is injected at port #B. The lines are guides for the eyes.

2.2. Dynamic characterization

After the static characterization, this section investigates the dynamic properties of the MZI-SOA. This study is focused on the properties of the MZI-SOA as an optical gate.

2.2.1. Experimental setup

Figure 13 shows the proposed setup to characterize the dynamic properties of the MZI-SOA. The setup follows the wavelength conversion design presented in Ref. [14], in a co-propagation design. This setup implements an all-optical exclusive OR (XOR) logical gate using a single MZI-SOA chip. From the MZI arms, both optical signals are launched into the SOAs, where their carrier densities and thereby the refractive index are modulated. This result in a phase modulation of the CW probe signal propagating through the SOAs by cross-phase modulation (XPM), according to the intensity variations of the input control signals. By carefully setting the input optical powers and controlling the SOA bias current, the control signal from the two SOAs interferes either destructively or constructively at the output of the MZI in order to provide the logical XOR operation of the two data sequences on the optical probe signal. From the XOR truth table, when both data signals injected at ports #D and #A are time synchronized, no pulses are observed on the probe signal at the MZI-SOA output (port #I). On the other hand, as the data signals give up time overlapping, some pulses with increasing intensity will appear on the probe signal, at the same MZI-SOA output.

The experimental setup consists of an external cavity laser peaking at 1549.32 nm (λ_1), followed by a polarization controller (PC) and an external Mach-Zehnder modulator (MZM). The non-return-to-zero (NRZ) data signal generated by a serial bit error rate tester (ref. Agilent N4901B) is then optically amplified by an erbium-doped fiber amplifier (ref. IPG-EAD-500-C3-W) and divided into two identical signals using a 50:50 coupler (COUPLER1) with symmetrical

outputs. Both optical signals coming from COUPLER1 are synchronized using optical delay lines. Polarization controllers are inserted on the light path to ports #D and #A of the MZI-SOA (ref. CIP 40G-2R2-ORP), to optimize the destructive interference at port #I. The probe signal, a CW light beam with 0 dBm and lasing at 1546.12 nm (λ_2), is launched into port #B of the MZI-SOA in a co-propagating direction with the data control signals. Different data patterns may be obtained by delaying signals at port #A and port #D. Finally, the probe signal is recovered at port #J, using a filter with a 40 GHz bandwidth (X-tract Net Test). The setup uses two instruments to analyse and measure the optical output signal: an optical complex spectrum analyser (OCSA) (APEX AP 2441A) to gather power and phase information of the output signal for time domain characterization and a sampling oscilloscope (Agilent 86100A) connected through a photodiode (HP-11982A).
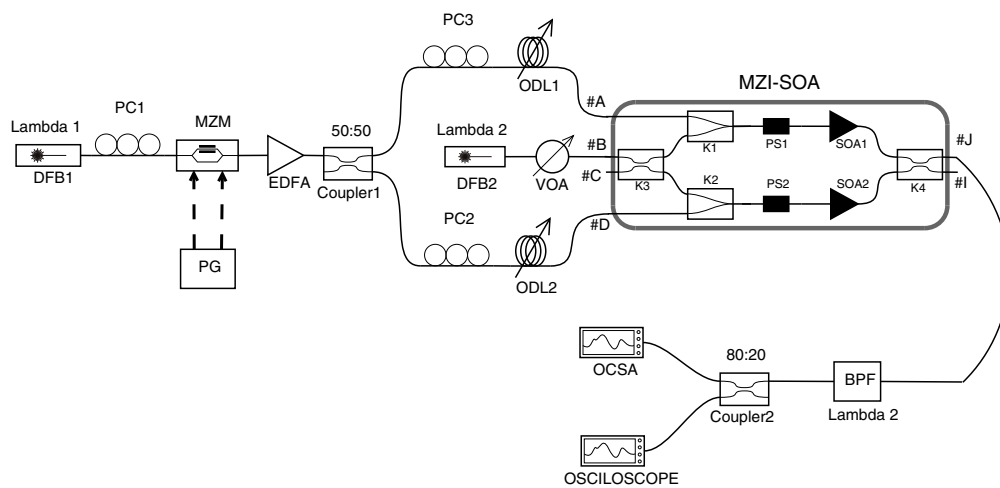

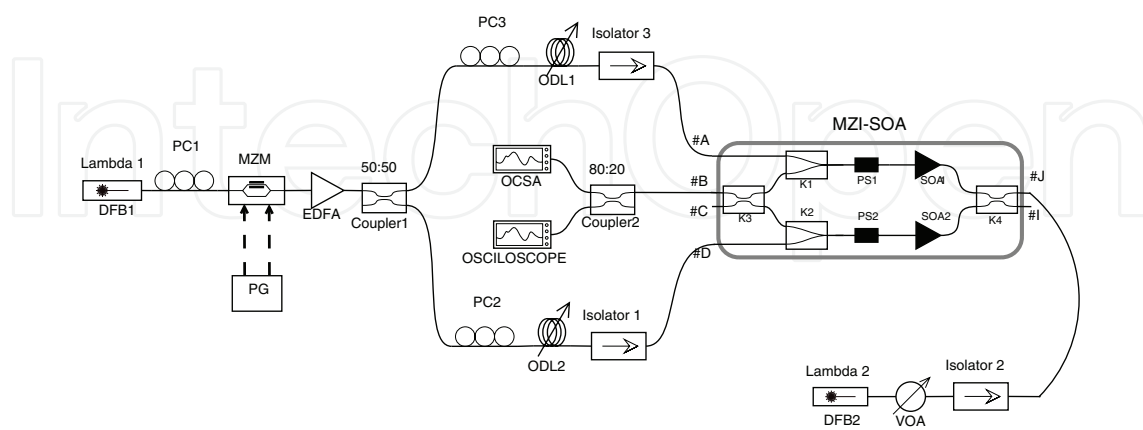**Figure 13.** All-optical XOR gate setup, based on a MZI-SOA, in a co-propagation scheme.

Figure 14. Wavelength and format conversion setup in counter propagation scheme.

The setup for the counter-propagation scheme uses the same probe signal, but now the signal is injected into port #I. As shown in **Figure 14**, the output signal is recovered at the constructive

interference output (port #B). An isolator is placed at ports #I, #D and #A to protect all laser sources from back propagation signals.

2.2.2. Experimental results and discussion

Figure 15 shows the data input signals (λ_1) injected into the arms #A and #D of the MZI-SOA, each with 2 dBm mean power, and the corresponding XOR gate output (λ_2), at 10 Gbps at port #J, in a co-propagating scheme. In this experimental scenario, the results are in conformity with the truth table of an XOR gate: the output presents a logical zero (0) if both the operands have identical value and a logical one (1) otherwise.
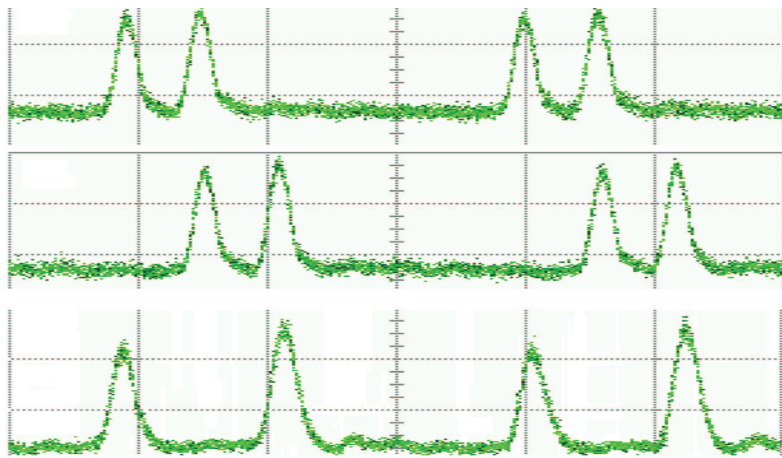

Figure 15. Optical sequences at MZI-SOA input ports #D and #A (first two signals from top) and resulting XOR output at port #J (bottom sequence). Horizontal scale: 500 ps/div. Vertical scale is arbitrary.
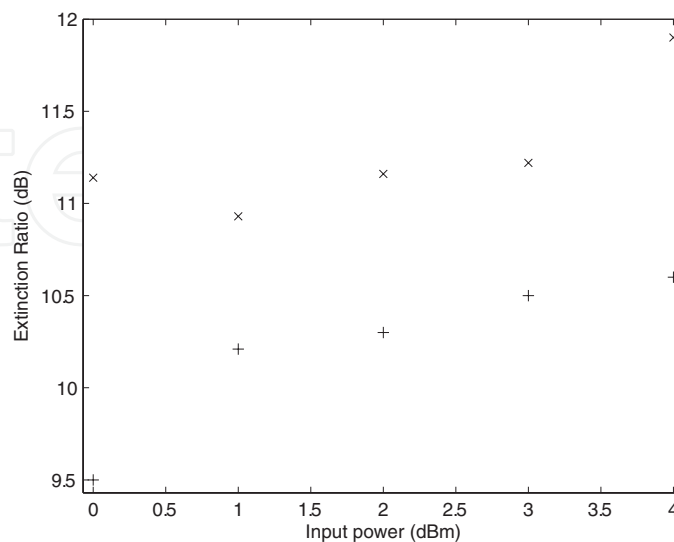

Figure 16. Experimental measurements of the ER of the output signal, as a function of the input power for co-propagation (+ sign) and counter-propagation (× sign) schemes.

Figure 16 shows the dependence of the ER at the output signal as a function of the power of the NRZ input signals, varying from 0 to 4 dBm. We set the CW probe signal power at 0 dBm. For both co- and counter-propagation proposals, we observe that changes on the input power do not affect the overall performance of the all-optical logical XOR gate, since the power variation of the two control signals involved in the assessment process is equivalent. But when compared with the co-propagation scheme, the counter-propagation scheme present better results, increasing the ER from 0.72 to 1.64 dB and improving the performance of the MZI-SOA as an optical gate. These results are in line with other experimental studies [15].

2.3. Summary

Having in mind next generation optical networks, which are meant to be as flexible and transparent as possible, this section has characterized the static properties and the operating conditions of the MZI-SOA working as an optical gate, which results will be useful for the following section, dealing with phase modulation and other advanced modulation format conversion techniques.

3. All-optical format conversion techniques

In the last two decades, the information volume flowing on communication networks increased exponentially, fostering the search for fast optical switching, gating and transmission techniques, along with equipment with integration facilities and low power consumption. Among those techniques, phase modulation of optical signals is an option that allows greater transmission distances in both analogue and digital transmission systems. Other method for more advanced modulation format conversion based on interferometric techniques will be also briefly described.

3.1. Format conversion from amplitude to phase modulation

Phase modulation generates signals with logical value 0 or 1, by varying the phase of light, while allowing it to be in the ON position. As opposed to intensity modulation, phase modulation has superior bandwidth efficiency and is not easily affected by signal distortions caused by relay nodes and transmission fibres. Several techniques have already been proposed to implement optical phase modulators, based on frequency shifters [16], lithium niobate (LiNbO$_3$) waveguide [17], gain transparent SOA [18] or using highly nonlinear fiber (HNLF) as the optical medium to phase modulate a CW laser [19].

Following the experimental findings with the XOR gate, this section characterizes the phase modulation properties of a MZI-SOA, using both interferometric arms, in co-propagation schemes. The setup is the same as the XOR gate of **Figure 13**, with MZI-SOA operational parameters (SOA bias current, input optical power) tuned to create a destructive output at port #I. When both control signals are synchronized, the optical CW coming out of the output of the two SOAs have opposite phases and interfere destructively when combined at COUPLER4. According to the XOR truth table in **Figure 17**, the resulting optical signal at port #I has no

observable amplitude variation [20]. Though, the phase ϕ of the probe signal λ_2 will vary in accordance to the input pattern, as depicted in **Figure 17** [21].
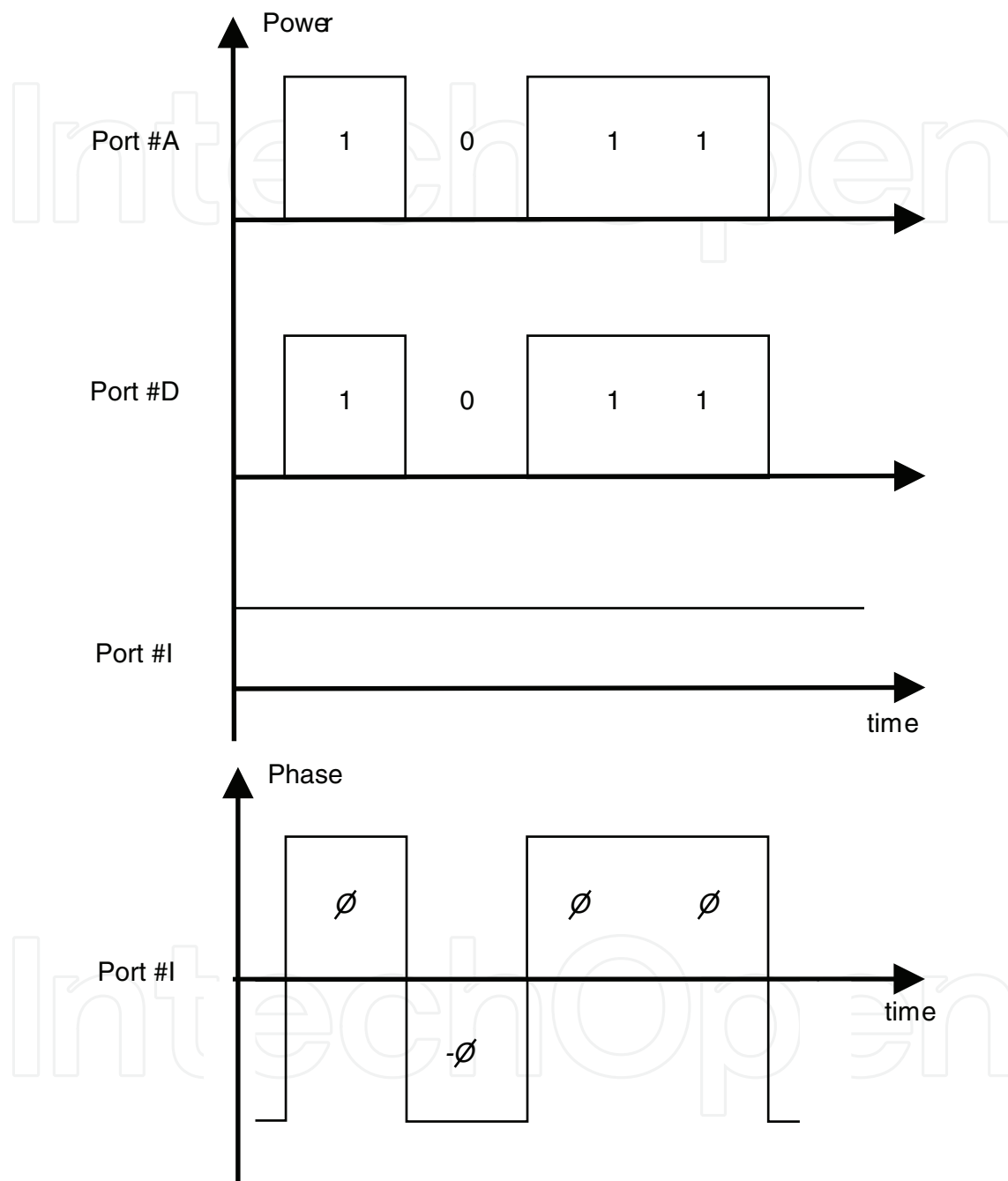

Figure 17. Principle of operation diagram of the conversion technique.

3.1.1. Experimental results and discussion

To investigate the phase modulation performance of an MZI-SOA for different bit rates, the operational parameters and the input power were optimized according to the phase eye

diagram opening, also called phase span in the subsequent paragraphs. BER measurements were not performed due to setup limitations imposed by the coherent receiver. The OCSA limits the size of the data sequence length to 4 bits at 2.5 Gbps or 16 bits at 10 Gbps [22], thus BER measurements are not feasible.

In order to confirm the feasibility of the interferometer as a phase modulator, experiments were carried out at bitrates of 2.5 and 10 Gbps. Data signals are launched into ports #D and #A with 2.5 dBm mean power and an average ER of 11.3 dB. The bias currents of both SOAs (I_{SOA}) were increased at the same time, from 150 to 300 mA at 2.5 Gbps and from 150 to 400 mA at 10 Gbps bit rate. For each bias value, the mean power of the control signal (P_{CW}) was swept from −6 to 2 dBm. The voltage applied to the PS was set to maximize the destructive interference at output port #I.

Figure 18 (left) presents a 4 bit pattern signal injected at ports #D and #A. **Figure 18** (right) shows the output signal at port #I, when control signal mean power is −4 dBm and SOA bias current is 250 mA. The phase variation associated to different logic levels is well pronounced but reversed when compared with the control signal intensity. Phase span and the mean power on the output signal are also proportional to the power of the CW probe signal and the bias current of the SOASs, as long as the SOAs are not in the saturated regime [9].
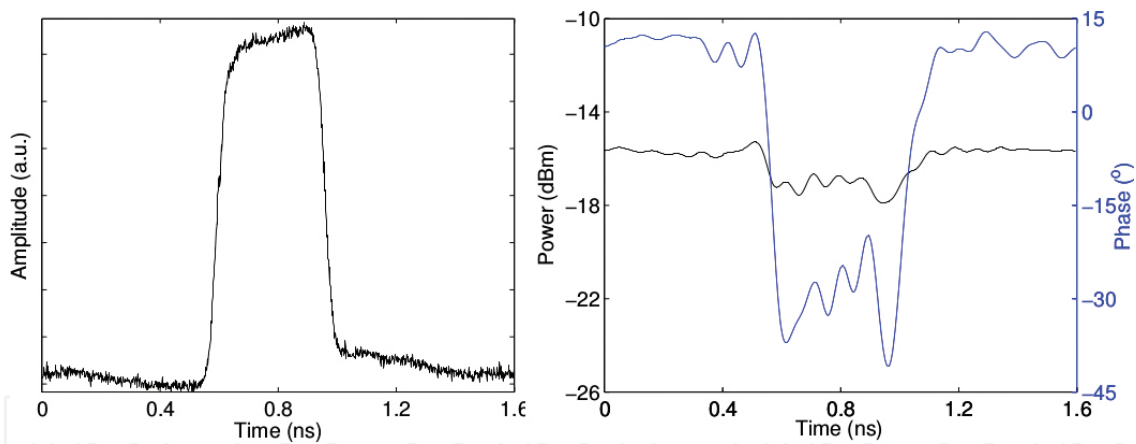

Figure 18. Left—Input sequence "0100"; Right—Phase and power output, with SOA input current I_{SOA} equal to 250 mA and input laser power P_{CW} equal to −4 dBm.

The proposed optical phase modulator was also characterized at 10 Gbps, and the tests were performed using data sequences 16 bits long [22]. **Figure 19** (left) shows the bit pattern launched at the input ports (#D and #A) of the interferometer. With SOA biased at 150 mA and control signal power launched at 0 dBm, the resulting output signal is depicted in **Figure 19** (right). Output power fluctuations are primarily due to noise. Similar to the previous experiments at 2.5 Gbps, phase shifts are inverted when compared with the logic levels of the data (control) signals. However, due to the carrier recovery time and the dynamics of the SOA, output phase levels are less pronounced at 10 Gbps when fast transitions occurs at the MZI-SOA input signals. Moreover, if the power of the probe signal is increased above 0 dBm, the

SOAs saturates and the conversion process is less efficient, which reduces the output mean power and phase span [9].
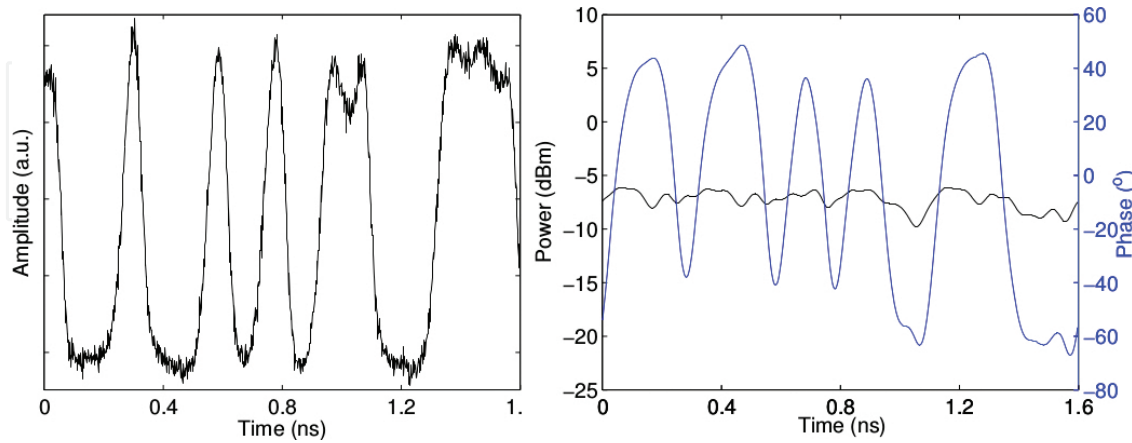

Figure 19. Left—Input sequence "1110010010101100"; Right—Phase and power output, with SOA input current I_{SOA} equal to 150 mA and input laser power P_{CW} equal to 0 dBm.

3.1.2. Summary

We have presented a method to perform optical phase modulation, from an all-optical XOR gate configuration. We measure the influence of input CW power and SOAs bias current on the signal phase at the MZI-SOA output port. We verify that an increase in the SOA bias current produces higher values of the mean power and the phase span of the output signal, but SOAs gain saturation has an inverse result on the same output signal. Overall, the experimental results show the viability of the MZI-SOA as device capable of all-optical modulation and format conversion.

3.2. Other advanced format conversions techniques

Higher order all-optical modulation formats can be generated using the phase modulator setup of **Figures 15** and **16** as a building block. For example, all-optical OOK to quadrature phase shift keying (QPSK) converter can be constructed with nested amplitude to binary phase shift keying (BPSK) converter pairs [23]. When the overall phase difference between the two nested BPSK pairs is set to $\pi/2$ rad, a QPSK signal is generated. Kang et al. [24] demonstrate the viability of this conversion scheme to generate a QPSK signal with 173 Gbps.

Furthermore, one may build a modulator for generating even higher order modulation formats, including quadrature amplitude modulation (QAM), following a similar method by which the amplitude to QPSK format converter is constructed [25]. Other methods of all-optical format conversion techniques using MZI-SOA are subject of further research in Ref. [26].

4. Conclusions

A MZI-SOA is a compact semiconductor device capable of performing many different all-optical modulations format conversion and generation functions. Its use has a building block for future all-optical networks can avoid the electronic bottleneck affecting opaque optical network nodes. It is estimated that 80% of the traffic flowing into a node is a pass-through traffic, with a destination located in another node of the network [27]. It is then particularly efficient to maintain that traffic flow in the optical domain, without optoelectronic conversion or packet processing. Transparent optical systems have the advantage of contributing to more energy-efficient networking without decreasing flexibility and agility. This clear and challenging objective is mandatory to cope with the traffic increase, while maintaining the cost and energy of the transported bit at an acceptable level.

Author details

Rogerio Pais Dionisio

Address all correspondence to: rdionisio@ipcb.pt

Escola Superior de Tecnologia, Instituto Politecnico de Castelo Branco, Castelo Branco, Portugal

References

[1] CISCO. The ZettabyteEra [Internet]. May 2012. Available from: http://www.cisco.com

[2] G. Wu, S. Talwar, K. Johnsson, N. Himayat and K. Johnson. M2M: from mobile to embedded internet. IEEE Communications Magazine. 2011;49(4):36–43.

[3] IEEE Communications Magazine. 2011;49(4):60–65.

[4] H. Karimi, M. Fenton, G. Lapierre, and E. Fournier. European Harmonized Technical Conditions and Band Plans for Broadband Wireless Access in the 790–862 MHz Digital Dividend Spectrum. In: IEEE, editor. Symposium on New Frontiers in Dynamic Spectrum; April 2010; Singapore. IEEE. 2010. pp. 1–9.

[5] Internet of Things [Internet]. July 2012. Available from: http://www.internet-of-things.eu/

[6] Celtic-Plus. Purple Book—Celtic Plus Programme of Possible and Recomended Research Items [Internet]. Available from: http://www.celtic-initiative.org/PurpleBook+/Purplebook.asp [Accessed: February 2012]

[7] CIP. CIP Technologies [Internet]. July 2012. Available from: http://www.ciphotonics.com/

[8] C. Reis, R. P. Dionisio, B. Neto, A. Teixeira and P. Andre. All-optical XOR based on integrated MZI-SOA with co- and counter-propagation scheme. In: IEEE, editor. ICTON Mediterranean Winter Conference; 10-12 December 2009; Angers, France. Warsaw, Poland: National Institute of Telecommunications. 2009. pp. 1–4.

[9] R. Dionisio, C. Reis, P. Andre, R. Nogueira and A. Teixeira. Experimental study of a phase modulator using an active interferometric device. In: IEEE, editor. MELECON 2010—15th IEEE Mediterranean Electrotechnical Conference; 26–28 April 2010; La Valleta, Malta; 2010. pp. 1142–1146.

[10] N. Yan, J. del Val Puente, T. G. Silveira, A. Teixeira, A. P. S. Ferreira, E. Tangdiongga, P. Monteiro and A. M. J. Koonen. Simulation and experimental characterization of SOA-MZI-Based multiwavelength conversion. Journal of Light wave Technology. 2009;27(2): 117–127.

[11] A theoretical and experimental study on modulation-format-independent wavelength conversion. Journal of Light wave Technology. 2010;28(4):587–595

[12] G. Maxwell, A. Poustie, C. Ford, M. Harlow, P. Townley, M. Nield, I. Lealman, S. Oliver, L. Rivers and R. Waller. Hybrid integration of monolithic semiconductor optical amplifier arrays using passive assembly. In: IEEE, editor. 55th Electronic Components & Technology Conference; 30 May–2 June 2006. Lake Buena Vista, Fl, USA. 2005. pp. 1349–1352.

[13] G. Maxwell, B. Manning, M. Nield, M. Hariow, C. Ford, M. Clements, S. Lucas, P. Townley, R. McDougall, S. Oliver, R. Cecil, L. Johnston, A. Poustie, R. Webb, I. Lealman, L. Rivers, J. King, S. Perrin, R. Moore, I. Reid and D. Scrase. Very low coupling loss, hybrid-integrated all-optical regenerator with passive assembly. In: IEEE, editor. European Conference on Optical Communication—ECOC 2002; 8–12 September 2002; Copenhagen, Denmark. 2002. pp. 1–2.

[14] T. Fjelde, D. Wolfson, A. Kloch, B. Dagens, A. Coquelin, I. Guillemot, F. Gaborit, F. Poingt and M. Renaud. Demonstration of 20 Gbit/s all-optical logic XOR in integrated SOA-based interferometric wavelength converter. Electronics Letters. 2000;36(22): 1863–1864.

[15] M. Hattori, K. Nishimura, R. Inohara and M. Usami. Bidirectional data injection operation of hybrid integrated SOA-MZI all-optical wavelength converter. IEEE Journal of Light wave Technology. 2007;25(2):512–519.

[16] B. Qi, L. L. Huang, H. K. Lo, and L. Qian. Polarization insensitive phase modulator for quantum cryptosystems. Optics Express. 2006;14(10):4264–4269.

[17] C. Langrock, E. Diamanti, R. V. Roussev, Y. Yamamoto, M. M. Fejer, and H. Takesue. Highly efficient single-photon detection at communication wavelengths by use of up

conversion in reverse-proton-exchanged periodically poled LiNbO3 waveguides. Optics Letter. 2005;30(13):1725–1727.

[18] W. Hong, D. Huang, X. Zhang, and G. Zhu. Simulation and analysis of gain-transparent SOA used as optical phase-modulator in DPSK applications. SPIE. 2007;6782:67.

[19] V. Marembert, C. Schubert, C. Weinert, H. G. Weber, K. Schulze, F. Futami and S. Watanabe. Investigations of fiber Kerr switch: nonlinear phase shift measurements and optical time division demultiplexing of 320 Gbit/s DPSK signals. In: Conference on Lasers and Electro-Optics CLEO 2005; 24–26 May 2005; Baltimore, USA. 2005. pp. 1432–1434.

[20] R. Vilar, J. M. Martinez, F. Ramos and J. Marti. All-optical DGD monitor for packet-switched networks based on an integrated active Mach-Zehnder interferometer operating as logic XOR gate. Optics Communications. 2008;281(21):5330–5334.

[21] S. C. Cao and J. C. Cartledge. Measurement-based method for characterizing the intensity and phase modulation properties of SOA-MZI wavelength converters. IEEE Photonics Technology Letters. 2002;14(11):1578–1580.

[22] APEX, editor. APEX Optical Spectrum Analyzer AP2041B. November 2009.

[23] K. Mishina, S. M. Nissanka, A. Maruta, S. Mitani, K. Ishida, K. Shimizu, T. Hatta and K. I. Kitayama. All-optical modulation format conversion from NRZ-OOK to RZ-QPSK using parallel SOA-MZI OOK/BPSK converters. Optics Express. 2007;15(12):7774–7785.

[24] I. Kang, M. Rasras, L. Buhl, M. Dinu, S. Cabot, M. Cappuzzo, L. Gomez, Y. Chen, S. Patel, N. Dutta, A. Piccirilli, J. Jaques, and C. Generation of 173-Gbits/s single-polarization QPSK signals by all-optical format conversion using a photonic integrated. In: ECOC 09—European Conference on Optical; September; p. 1.

[25] R. Dionisio, R. Nogueira and A. Teixeira. Advanced optical modulation and format conversion. In: SPIE, editor. AOP 2013—Conference on Application of Optics and Photonics; 26 May 2014; Aveiro, Portugal. doi:10.1117/12

[26] R. Dionisio, R. Nogueira and A. Teixeira. Parametric impairments analysis of all-optical format conversion techniques with MZI-SOA. In: SPIE, editor. Conference on Application of Optics and Photonics; 26 May 2014; Aveiro, Portugal. 2014. doi:10.1117/12

[27] Y. Zhang, P. Chowdhury, M. Tornatore, and B. Mukherjee. Energy efficiency in telecom optical networks. IEEE Communications Surveys Tutorials. 2010;12(4):441–458.